

Article

Not peer-reviewed version

---

# An Open-Source Retrospective Analysis of Hypertrophic and Dilated Cardiomyopathy Using Machine Learning and Electrocardiogram Data

---

Arda Altintepe and [Asu Rustemli](#)\*

Posted Date: 23 January 2026

doi: 10.20944/preprints202601.1815.v1

Keywords: electrocardiogram (ECG); vectorcardiogram (VCG); machine learning; dilated cardiomyopathy; hypertrophic cardiomyopathy; obstructive hypertrophic cardiomyopathy; ischemic dilated cardiomyopathy



Preprints.org is a free multidisciplinary platform providing preprint service that is dedicated to making early versions of research outputs permanently available and citable. Preprints posted at Preprints.org appear in Web of Science, Crossref, Google Scholar, Scilit, Europe PMC.

Copyright: This open access article is published under a [Creative Commons CC BY 4.0 license](#), which permit the free download, distribution, and reuse, provided that the author and preprint are cited in any reuse.

Disclaimer/Publisher's Note: The statements, opinions, and data contained in all publications are solely those of the individual author(s) and contributor(s) and not of MDPI and/or the editor(s). MDPI and/or the editor(s) disclaim responsibility for any injury to people or property resulting from any ideas, methods, instructions, or products referred to in the content.

Article

# An Open-Source Retrospective Analysis of Hypertrophic and Dilated Cardiomyopathy Using Machine Learning and Electrocardiogram Data

Arda Altintepe<sup>1</sup> and Asu Rustemli<sup>2,\*</sup>

<sup>1</sup> Horace Mann School, USA

<sup>2</sup> Ocean Cardiovascular, LLC, USA

\* Correspondence: asurustemli@gmail.com

## Abstract

**Background/Objectives:** Dilated (DCM) and hypertrophic cardiomyopathy (HCM) are common cardiomyopathies associated with heart failure. Electrocardiogram (ECG) screening before an echocardiogram could help streamline diagnosis, particularly in rural areas. Prior ECG machine-learning (ML) studies do not use open-source data when studying cardiomyopathy, and very few proprietary studies directly compare HCM and DCM or address ECG differences within obstructive (HOCM) and non-obstructive HCM (HNCM). **Methods:** Standard and vectorcardiogram-derived (VCG) ECG features were extracted from the MIMIC-IV-ECG database. The final cohort comprised 599 patients (HCM = 208 [HOCM = 99, HNCM = 53, unknown = 56], DCM = 391 [ischemic cardiomyopathy with left ventricular dilation = 250, non-ischemic = 141]). Logistic regression (LR) and extreme gradient boosting (XGBoost) with five-fold cross-validation separated HCM from ischemic cardiomyopathy with left ventricular dilation (DCM-I) and non-ischemic DCM (DCM-NI), and HOCM from HNCM. **Results:** Using the area under the receiver operating characteristic curve (AUC-ROC) as the performance metric, LR achieved high discrimination of HCM from DCM-I (0.92) and DCM-NI (0.90). However, differentiating HOCM from HNCM proved more difficult (XGBoost = 0.81; LR = 0.75). Both DCM subtypes (especially ischemic) showed lower QRS amplitudes and right-posterior ventricular gradient orientation; HCM displayed higher amplitudes and larger, more complex T-loops. Within HCM, HOCM had stronger leftward electrical activity and more dipolar to non-dipolar QRS energy after singular value decomposition. **Conclusions:** Using only open-access data, we demonstrate an interpretable ECG-based pipeline that discriminates cardiomyopathy and highlights distinct features. While detecting obstruction remains difficult, ECG features provide measurable separation, supporting possible diagnostic screening and offering a reproducible framework for future studies.

**Keywords:** electrocardiogram (ECG); vectorcardiogram (VCG); machine learning; dilated cardiomyopathy; hypertrophic cardiomyopathy; obstructive hypertrophic cardiomyopathy; ischemic dilated cardiomyopathy

## 1. Introduction

Cardiomyopathy (CM) describes a diverse group of diseases affecting the heart muscle. [1] Dilated cardiomyopathy and hypertrophic cardiomyopathy represent the two most common forms of CM with the highest risk of heart failure and sudden cardiac death [1]. In dilated cardiomyopathy (DCM), the ventricular chambers enlarge, and the heart's pumping ability weakens, reducing stroke volume and impairing systolic function [1,2]. DCM can develop from causes such as genetic mutations, myocarditis, or toxic exposures like alcohol. Whereas ischemic injury due to chronic artery disease can cause left ventricular systolic dysfunction with or without regional wall motion abnormalities. In some cases, there may be left ventricular dilation, for which those patients could

morphologically be considered ischemic dilated cardiomyopathy. In hypertrophic cardiomyopathy (HCM), the ventricular walls thicken abnormally, often causing impaired diastolic filling and in some cases dynamic outflow obstruction [1–3,10]. Unlike DCM, HCM usually occurs because of inherited genetic changes in the heart muscle proteins [1,2].

The treatments of DCM and HCM are distinctive. Thus, early diagnosis is imperative to determine the correct treatment, halt the progression of DCM, limit symptoms, and improve prognosis [2]. Diagnosis is traditionally done through imaging studies such as echocardiography and magnetic resonance imaging (MRI) [2]. Currently, the most widely available diagnostic tool is an echocardiogram. However, echocardiograms may not be as practical in rural areas or developing countries due to the high cost or lack of infrastructure and well-trained cardiac sonographers [3]; the electrocardiogram (ECG) may present an inexpensive and noninvasive screening approach before conducting an echocardiogram. Vectorcardiography (VCG) extends this concept by transforming the ECG into a three-dimensional representation of the heart's electrical activity. Instead of looking at each lead separately, VCG traces the overall direction and magnitude of the instantaneous heart vector in 3D space. This approach can highlight patterns of depolarization and repolarization that standard ECG features may miss, offering additional discriminatory power for cardiomyopathy diagnosis. This study explores the capabilities of ECGs as well as their VCG representations to differentiate HCM, DCM, and several phenotypes.

Studies on artificial intelligence (AI) and machine learning (ML) have recently demonstrated potential in classifying cardiomyopathy [4–8], which could prove useful in diagnosis. However, most studies use echocardiograms. For example, R. Nasimov created a convolutional neural network (CNN) to classify DCM from HCM based on echocardiogram imaging, reaching an accuracy of 96.6% [4]. Zhou et al present an echo-based XGBoost algorithm with a 0.93 to classify Ischemic Cardiomyopathy from Dilated Cardiomyopathy [5]. Machine learning and deep learning models that identify hypertrophic cardiomyopathy from ECG data also exist; Ko and Attia constructed a deep-learning convolutional neural network to identify HCM from non-HCM patients with an AUC of 0.96 [6]. Kokubo et al. offer deep-learning models with acceptable accuracies to detect left ventricular dilation and left ventricular hypertrophy from ECG waveforms [7]. Yet, left ventricular hypertrophy and left ventricular dilation are only common features of HCM and DCM patients, respectively; their presence alone cannot be used to diagnose CM [8]. A recent study highlighted advanced ECG (A-ECG) features derived from vectorcardiogram (VCG) transformations, which achieve high accuracy in identifying patients with non-ischemic or ischemic cardiomyopathy, apical HCM, and asymmetric septal HCM within a broader cohort comprised of healthy individuals and those with other cardiac diseases [9]. Their ischemic and non-ischemic cardiomyopathy groups were defined by reduced left ventricular ejection fraction (LVEF) rather than explicit left ventricular dilation criteria; therefore, these categories may not correspond to DCM (dilation and dysfunction). Their primary focus was apical HCM (and further subtype) detection rather than ECG feature comparisons for HCM vs DCM.

Approximately one-third of patients with HCM develop dynamic left-ventricular outflow-tract obstruction (LVOTO). Resting LVOTO is a strong, independent predictor of progression to severe heart-failure symptoms and of sudden cardiac death [10]. Obstructive HCM (HOCM) requires negative inotropic drugs, and patients with HOCM may need invasive therapies such as septal reduction. Identifying LVOTO without ultrasound imaging remains challenging. A 2023 cross-sectional study of 200 HCM patients reported that standard surface ECG variables could not reliably separate HOCM from non-obstructive HCM (HNCM) [11]. This negative result highlights a diagnostic gap that advanced ECG analytics might fill. Guo et al. prospectively developed and externally validated a logistic-regression model using only two standard ECG parameters (P-wave interval and SV1) that differentiated HOCM from HNCM with C-statistics of 0.805 in a temporal validation cohort and 0.776 in an external cohort [12]. To our knowledge, apart from a single pragmatic model by Guo et al., no peer-reviewed study has demonstrated meaningful ECG-based discrimination of obstructive versus non-obstructive HCM.

Additionally, no prior study to date has relied on publicly available data for ECG-based cardiomyopathy diagnosis. The use of open-source datasets presents unique challenges, as these datasets are typically not curated for the specific task and often lack reliable labels and standardized data structures. In contrast, reliance on proprietary datasets restricts reproducibility and broad access within the research community. The Medical Information Mart for Intensive Care IV is a large deidentified dataset of patients admitted to the emergency department or an intensive care unit at the Beth Israel Deaconess Medical Center in Boston, MA [13–15]. The dataset is open-access and available on PhysioNet. In this study, we explore the possible applications of using open-source data with advanced feature analysis to quantify ECG discriminatory ability within cardiomyopathy and its functional phenotypes. Specifically, we run statistical tests and develop machine-learning models to separate hypertrophic cardiomyopathy from both ischemic and non-ischemic dilated cardiomyopathy and also detect LVOT obstruction within hypertrophic cardiomyopathy.

## 2. Materials and Methods

### 2.1. Patient Cohort

All data were from the Medical Information Mart for Intensive Care (MIMIC)-IV, a large deidentified dataset of patients admitted to the emergency department or an intensive care unit between 2008 and 2022 at the Beth Israel Deaconess Medical Center in Boston, MA [13]. Hospital admissions with International Classification of Diseases (ICD) 9 and 10 discharge codes related to dilated cardiomyopathy (DCM), ischemic cardiomyopathy (ICM), and hypertrophic cardiomyopathy (HCM) were mapped to patient IDs and demographic information. ICD codes “I420,” “I426,” “4255,” and “4257” were used for dilated cardiomyopathy, while “I255” was used for ischemic cardiomyopathy, and “I421,” “I422,” “4251,” “42511,” and “42518” were used for hypertrophic cardiomyopathy. For at least one hospital admission, 701 patients were given a DCM code, 1,527 were given an ICM code, and 522 were given an HCM code. The MIMIC-IV-ECG module was then used to map electrocardiograms to patients in the cohort [16]. We only included patients with an ECG taken during their hospital stay of diagnosis, retaining 2,003 unique patients, or 73% of the cohort. ECGs with paced rhythms, artifact ECGs, bundle branch blocks, left anterior fascicular or posterior blocks, intraventricular conduction defects, prominent premature ventricular contractions, atrial fibrillation, or atrial flutter were excluded from the study, fully removing 421 patients.

However, upon manual review of the discharge notes for several corresponding admissions located in the MIMIC-IV-Note module [17], many ICD diagnoses did not match the physician-written discharge report for the admission. For example, the HCM ICD codes for “obstructive hypertrophic cardiomyopathy” and “other hypertrophic cardiomyopathy” commonly also did not align with whether the LVOT gradient was truthfully obstructive, as indicated in the discharge notes. Also, from just ICD codes, there is no way to tell whether an ICM-coded patient also has LV dilation. Many stays did not have an echocardiogram taken during their hospital admission, and these stays could not be trusted to provide an accurate label.

To create more reliable diagnosis labels without relying on closed-source expert review, the GPT-4.1 large language model (LLM) was chosen for direct text classification [18], as its flexibility handles the heterogeneity of discharge reports far better than conventional rule-based natural language processing pipelines. Temperature was set to 0 to ensure reproducibility. In the first call, the LLM was instructed to carefully read a discharge report and assign HCM, DCM (echo criteria was reduced LVEF and LV dilation, including ICM with LV dilation), or neither based strictly on current echocardiogram criteria and explicit physician documentation. The model functioned as an information extractor rather than a clinical decision-maker. A numerical left ventricular ejection fraction (LVEF) was also extracted when reported, which could be used for further purposes. Most discharge notes were classified as neither, which included ambiguous cases or those that specified ischemic or alcoholic cardiomyopathy without echocardiogram-supported LV dilation. For admissions labeled HCM, another call was made with the purpose of extracting clear current-

echocardiogram-verified LVOT obstruction (HOCM vs HNCM vs unknown) and whether a septal reduction procedure (myectomy or alcohol ablation) occurred during the admission. For admissions labeled DCM, the model classified ischemic status (ischemic vs non-ischemic vs unknown) based on clear documentation of coronary artery disease, myocardial infarction, revascularization, or explicit ischemic diagnostic terms. Unknown DCM cases were dropped. For each classification step (both the primary HCM vs. DCM distinction and the subsequent subtype assignments) the model provided direct quotes from the text supporting the final decision.

The derived labels and supporting excerpts have been submitted to PhysioNet for dissemination under credentialed access and are currently under review. All non-“neither” final diagnoses were reviewed to be consistent with the underlying clinical text. Two examples of incorrect ICD diagnoses with corrected GPT-4.1-derived diagnoses are shown in Figure 1.

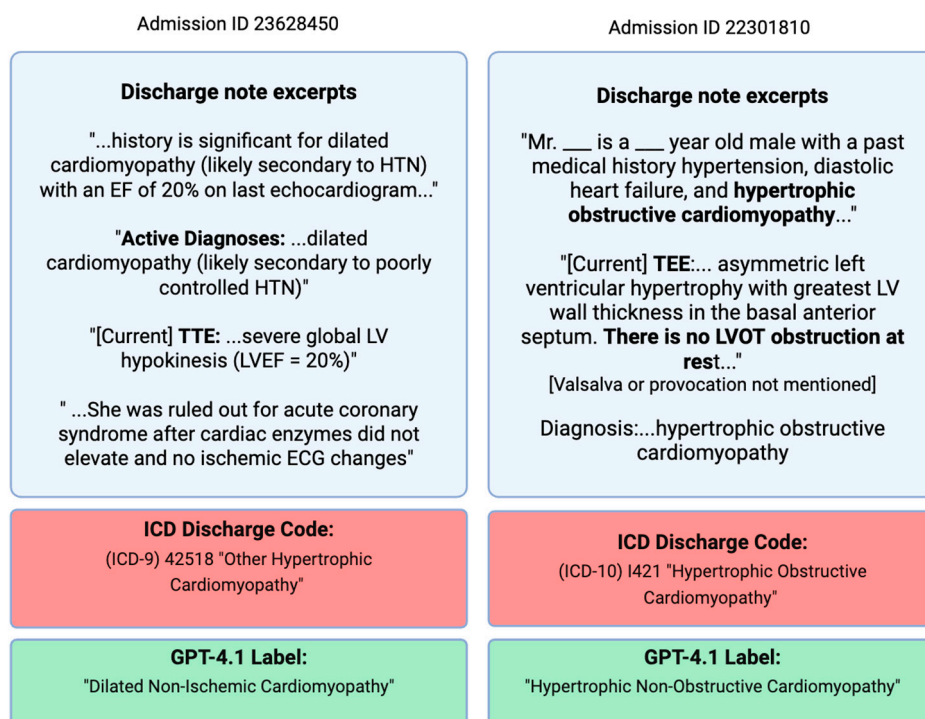


**Figure 1.** Two discharge notes from unique patients with corresponding ICD and final GPT-4.1 labels for their hospital visit. The patient on the left presents with clear non-ischemic DCM but received an incorrect HCM diagnosis code, which was later corrected by GPT-4.1. On the right, the patient is indicated to have a history of HOCM and received an HOCM diagnosis. However, the echocardiogram findings from the hospital visit directly indicate no LVOT obstruction with no mention of valsalva obstruction, so the patient should be labeled HNCM. This was correctly done by GPT-4.1, which gives full emphasis to the current echocardiogram.

208 patients with hypertrophic cardiomyopathy (99 obstructive, 53 non-obstructive), and 391 patients with dilated cardiomyopathy (250 ischemic, 141 non-ischemic) remained in the final cohort. DCM-I refers to ischemic cardiomyopathy with left ventricular dilation. One ECG was kept per patient, and priority was given to clean ECGs with a definitive phenotype label (not HCM unknown). Morphological HCM phenotypes, including septal and apical variants, were eventually not considered due to the lack of specification in the reports and minimal sample size. Figure 1 shows the full filtering history of the cohort.

## 2.2. ECG Feature Extraction

Each ECG wave measures electrical impulses during the stages of a heartbeat. The Waveform Database Software Package was used to convert the waveforms sampled at 500hz into a data frame

showing time in milliseconds and amplitude for each lead [19]. Neurokit2, an open-source toolbox for physiological signal processing, was used to clean and determine the locations of most onsets, peaks, and offsets of Q, R, S, T, and P waves for each remaining ECG (illustrated in Figure 2) [20]. The “prominence” method proposed by Emrich et al was used for delineation [21]. Delineation was done for each of the 12 ECG leads, which represent different electrical views obtained from the anterior chest and limbs.

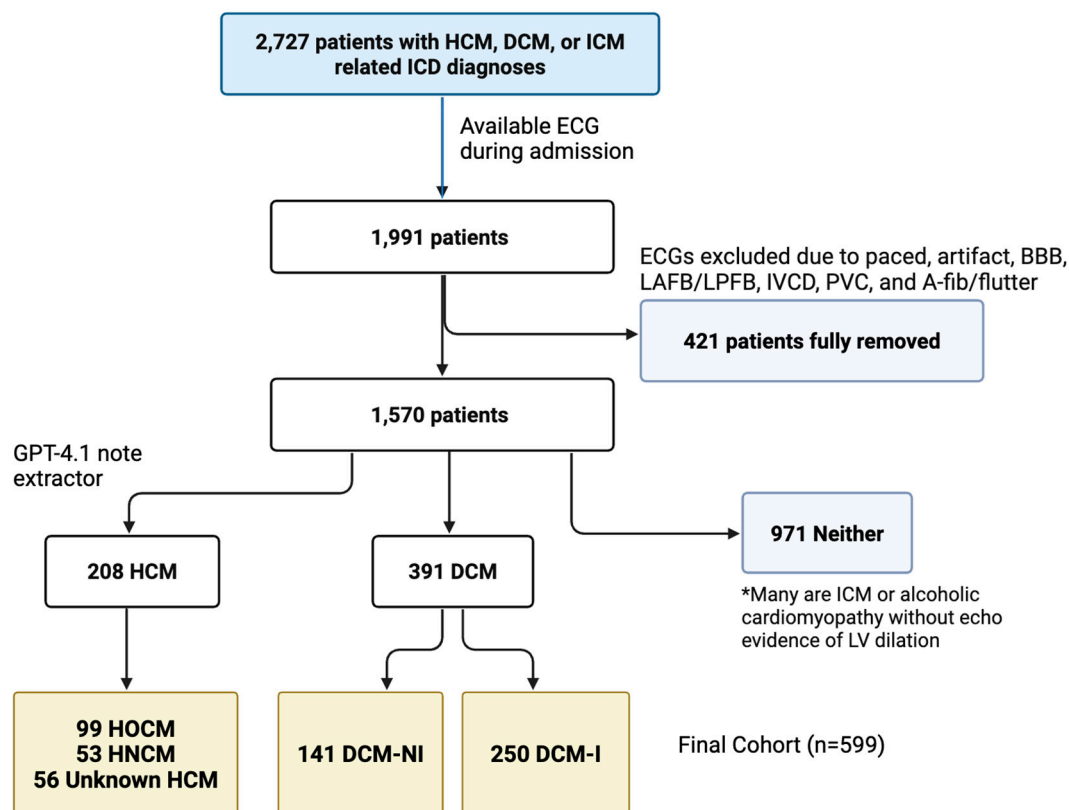


Figure 2. Flow chart showing the study population.

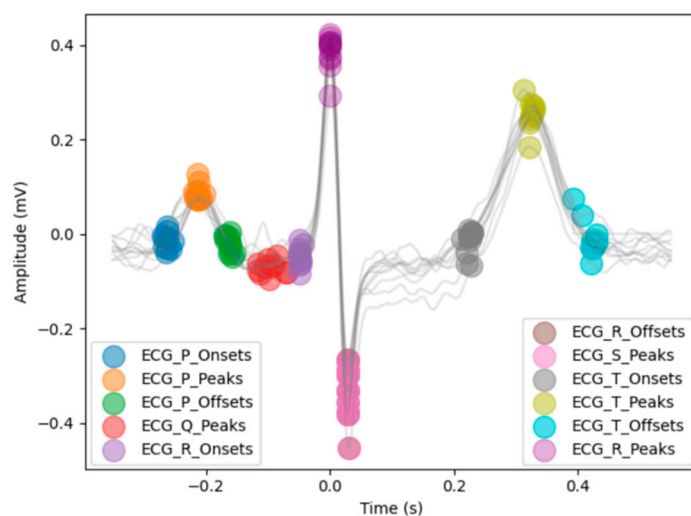


Figure 3. Visual of all detected peaks, onsets, and offsets for a sample lead II in the study population using “prominence”. Heartbeats and ECG markers from the 10-second lead II are overlaid. Time (s) is relative to the location of R peaks. The example S-peak and R-offset markers are stacked at the same location. Notice there are no Q-onsets or S-offsets provided in “prominence”.

Median peak amplitudes were calculated for each wave in reference to the isoelectric PR baseline, as well as intervals and wave durations. ECG waveforms were also transformed using Fourier analysis to extract power-spectral and higher-order statistical moment features for each lead, with an example being the mean frequency in lead V1 (Hz) or the time-domain kurtosis in lead V3.

### 2.3. Vectorcardiogram Feature Extraction

A 3D vectorcardiogram representation of an ECG can be built from eight linearly independent leads (I, II, V1, V2, V3, V4, V5, and V6), and having fixed global P, QRS, and T intervals from the standard ECG allows for the construction of P, QRS, and T loops in the VCG projection. Because “prominence” delineation does not locate Q-onsets and S-offsets by default, we developed an automated pipeline using discrete wavelet transform delineation and further amplitude threshold checks to ensure a full QRS-interval selection algorithm. The P, QRS, and T-wave intervals relative to their R-peaks in each of the eight independent leads were combined into a fixed global median. The median was then applied onto a mean heartbeat for each lead. The mean heartbeats were constructed using the R-peak indices of lead V5, to ensure consistent temporal indices throughout all peaks using a reference lead with clear and large R-waves. A Kors regression matrix transformation projected eight 850-ms mean heartbeats into a 3D VCG space [22]. Using the fixed global P, QRS, and T-wave windows, the analyzed VCG features included peak spatial magnitude, loop geometry, ventricular-activation time, time-voltage area, QRS-T angles, ventricular-gradient strength and direction, and other amplitude or area-based features that describe cardiac depolarization and repolarization.

Finally, all derived ECG features were concatenated with features provided from MIMIC-IV ECG machines: 7 global numerical measurements, including QRS duration and axis, as well as 11 Boolean ECG features such as “left ventricular hypertrophy” extracted from MIMIC-IV machine-generated report text. The total feature set included 14 lead-specific amplitude and Fourier-based features, 30 global interval and axis-based features, 11 Boolean summary features, and 41 VCG-derived features.

### 2.4. Machine Learning Model

Two machine-learning algorithms were trained to assess the discriminatory ability between hypertrophic and dilated cardiomyopathy phenotypes across three binary classification tasks: HOCM vs. HNCM, HCM vs. DCM-NI, and HCM vs. DCM-I. The first model trained for each task, multivariate logistic regression (LR), uses a linear combination of predictors, fitted with the liblinear solver (L1 penalty,  $C = 0.1$ ). Since LR cannot handle missing data, for HCM vs. DCM-I and DCM-NI, all features were used as inputs, and the three features with the most missing values were dropped. All rows with remaining missing values were subsequently excluded. We also trained an extreme gradient boosting (XGBoost) model, a non-linear ensemble method that builds decision trees sequentially and re-weights misclassified samples to improve performance. XGBoost can natively handle missing values. For HOCM vs. HNCM, the 10 features with the highest discriminatory ability were chosen as model inputs, and any rows with missing values in those features were dropped. Models were implemented in Scikit-learn (v1.5.1). Performance was estimated with 5-fold stratified cross-validation using out-of-fold probabilities. We report the area under the receiver-operating-characteristic curve (AUC-ROC), which summarizes rank discrimination across thresholds, and the area under the precision-recall curve (AUC-PR), which gives a balanced estimate of performance under class imbalance. We also report sensitivity and specificity calculated at the threshold maximizing Youden’s J statistic.

### 3. Results

#### 3.1. HOCM vs. HNCM: Feature Differences

Obstructive and non-obstructive HCM were compared across all ECG variables. Fourteen representative variables that met the significance threshold ( $p < 0.05$ ) are summarized in Table 1; the full set of variables meeting  $p < 0.05$  is provided in Table S1. In Table 1, variables are listed with median [IQR, interquartile range] for each group, the effect size (Cliff's delta or risk difference), and the  $P$  value (Mann-Whitney U test). Lead names and units are included in the variable label; for amplitude features, SaVR, for example, denotes the median absolute value of the S-wave amplitude in lead aVR measured from the prior isoelectric PR baseline. QRS onset and end are global MIMIC-IV numerical measures from a representative heartbeat. Figure 4 shows kernel density estimates (KDEs) for three ECG features.

**Table 1.** An ordered list of 14 chosen ECG variables that differed significantly ( $p < 0.05$ ) between hypertrophic obstructive and non-obstructive phenotypes.

ECG Feature	HOCM (n=79)	HNCM (n=53)	Effect size	$P$
SV1 (mV)	0.86 [0.60, 1.27]	0.66 [0.31, 0.94]	0.283	.004
SII (mV)	0.07 [0.03, 0.20]	0.15 [0.06, 0.30]	-0.299	.002
RV2 (mV)	0.18 [0.08, 0.36]	0.29 [0.13, 0.62]	-0.284	.004
RV6 (mV)	0.88 [0.52, 1.18]	0.66 [0.35, 0.83]	0.316	.001
R/S amplitude ratio (II)	10.87 [2.70, 22.02]	2.63 [1.20, 7.27]	0.357	<.001
R/S amplitude ratio (aVR)	0.18 [0.08, 1.09]	1.04 [0.29, 1.54]	-0.333	<.001
QRS end (ms)	296.00 [274.00, 325.00]	326.00 [292.50-359.50]	-0.309	.002
P duration (ms)	108.00 [98.50, 119.50]	120.00 [102.00, 128.50]	-0.286	.018
Time-domain skewness (V1)	-2.97 [-3.42, -2.48]	-2.62 [-3.24, -1.08]	-0.290	.004
R amplitude in lead Y (mV)	0.35 [0.15, 0.66]	0.19 [-0.08, 0.40]	0.289	.003
Spatial P-QRS mean-vector angle (°)	91.58 [65.38, 124.25]	68.89 [48.25, 100.51]	-0.246	.012
QRS-T eigenvector-1 angle (°)	42.68 [15.49, 122.53]	67.35 [25.87, 153.79]	-0.228	.025
Normalized QRS eigenvector-2	0.32 [0.21, 0.49]	0.44 [0.31, 0.59]	-0.257	.009
ln QRS non-dipolar to dipolar ratio	-1.26 [-1.61, -1.02]	-1.04 [-1.33, -0.91]	-0.272	.006

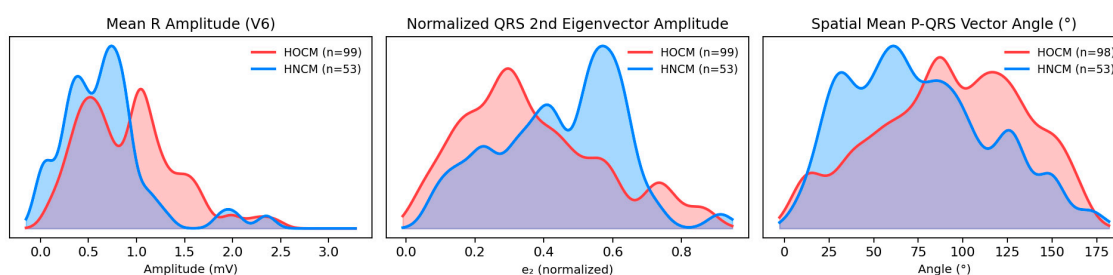


**Figure 4.** Kernel Density Estimate (KDE) plots of three ECG-derived features between obstructive and non-obstructive hypertrophic cardiomyopathy. One HOCM patient did not have valid P-loop detected in the VCG feature extraction.

#### 3.1.1. Amplitude and Interval Findings

R/S amplitude ratios were consistently higher in HOCM across all left-lateral leads (I, aVL, V5–V6) and all inferior leads (II, III and aVF), while HNCM showed higher ratios in the rightward leads (aVR and the right precordials V1–V2) (all  $P < .05$ , Table S1). Because the RS ratio increases with a larger positive R wave and a smaller negative S wave, a higher ratio indicates greater net depolarization along that lead's axis. In lead V6, the mean R-amplitude was 0.88 [0.52-1.18] in HOCM and 0.66 [0.35, 0.83] in HNCM (Table 1 and Figure 4). Temporally, in a representative heartbeat starting 40 ms before the representative P-onset, the QRS-end occurred later in non-obstructive HCM

patients. The P duration was also longer in HNCM, lasting a median 120 ms compared to 108 ms in HOCM.

### 3.1.2. Vectorcardiogram Findings

For the VCG-derived features, HNCM had a higher normalized amplitude for the second QRS eigenvector (the ratio of the second to first singular of the QRS-loop [ $\sigma_2/\sigma_1$ ]). The total QRS non-dipolar to dipolar ratio ( $(\sigma_2 + \sigma_3) / \sigma_1$ ) was also higher in HNCM (Figure 4 and Table 1). Thus, in comparison to the dominant axis, the second and third orthogonal axis captured more energy during depolarization, meaning depolarization was less planar or spatially uniform in HNCM. Additionally, the angle between the mean spatial P and QRS vectors was larger in HOCM, while the angle between the first QRS and T eigenvector was larger in HNCM (Figure 4).

### 3.2. HCM vs. DCM: Feature Differences

**Table 2.** Displays demographic data within cardiomyopathy. Age is expressed as median [IQR]. Sex and race are shown as percentages (frequency).

Feature	DCM-NI (n=141)	DCM-I (n=250)	HCM (n=208)
Age (years)	56.00 [47.00, 64.00]	69.00 [60.00, 78.00]	67.00 [57.00, 79.25]
Male	80.9% (114)	76.0% (190)	46.2% (96)
Black	34.8% (49)	9.6% (24)	17.3% (36)
Hispanic	6.4% (9)	5.2% (13)	4.8% (10)
White	44.0% (62)	70.0% (175)	63.0% (131)

DCM-NI was younger (median 56y) than DCM-I (69y) and HCM (67y), and both DCM-NI and DCM-I were predominantly male (~81% and 76%) compared with HCM (~46% male). Race distributions varied, with DCM-NI comprising a higher proportion of Black patients (~35%) and DCM-I a higher proportion of White patients (70%).

All amplitude, duration, Fourier, and VCG-derived features were also tested for significance within the DCM-NI, DCM-I, and HCM (obstructive, non-obstructive, and unknown together). 500 electrically normal ECGs were also included for visual comparison, but not included within statistical tests. A full table containing all features is available in Table S2.

HCM was found to have the highest QRS amplitudes throughout all leads, with particularly large R-wave amplitudes in limb leads (Table S2). For example, the median R-wave amplitude in lead I was 0.76 mV for HCM, 0.51 mV for DCM-NI, 0.41 mV for DCM-I, and 0.55 mV for the electrically normal cohort (Table S2 and Figure 5). Throughout precordial leads, DCM-I displayed especially low amplitudes: in V5, the median R-wave amplitude for DCM-I was only 0.39 mV, in comparison to 0.76 mV in DCM, 0.80 mV in HCM, and 0.84 mV for normal ECGs. HCM also had the largest maximum amplitude of the spatial QRS vector at 1.15 mV, in comparison to 1.08 mV for DCM-NI, 0.86 mV for normals, and 0.85 mV for DCM-I. DCM-I consistently showed time-domain skewness closer to zero and lower kurtosis for most leads, indicating lower overall amplitudes, broader durations, and more symmetric waveforms. T-waves were flatter in both DCM (low spatial max-to-mean vector ratio).

As referenced in Table S2, the QRS duration was longest in DCM-I (107 ms vs 86 ms in normals). While also having longer QRS durations, non-ischemic dilated cardiomyopathy displayed shortened repolarization durations, primarily in the terminal phase. The median T-wave duration in DCM-NI was around 35 ms shorter than normal, with the downslope alone being over 30 ms shorter. While the duration was not corrected for the shorter RR interval (median 681 ms), the upslope of the T-wave was still over twice as long as the downslope (T index 2.24) in DCM-NI, compared to a ratio of only 1.13 and 1.27 for normals and HCM. 27% of DCM-NI patients compared to only around 12% of both HCM and DCM-I had sinus tachycardia rhythms.

Compared with dilated cardiomyopathy (ischemic and non-ischemic) and electrically normal ECGs, hypertrophic cardiomyopathy showed both greater T-loop energy and spatial complexity. The

first T-loop singular value (log dipolar T-wave amplitude) was largest in HCM (median  $-0.01$ ) vs DCM-NI ( $-0.58$ ) and DCM-I ( $-0.53$ ), with normals near  $-0.04$  (Table S2 and Figure 5). The second T-loop singular value, a marker of non-planarity, was also larger in HCM ( $-1.39$ ) than in DCM ( $-1.75$ ) and DCM-I ( $-1.67$ ), with normals at  $-1.77$  (Table S2). Multiple directional VCG metrics highlighted distinct abnormalities in dilated cardiomyopathy (both ischemic and non-ischemic), showing very similar right-posterior orientation shifts, while HCM remained closer to normal. For the ventricular gradient (VG)—the spatial integral of the instantaneous heart vector over depolarization and repolarization—the median sine of the azimuth angle in the sagittal plane were  $0.86$  (DCM-NI) and  $0.87$  (DCM-I) versus  $0.31$  (HCM) and  $-0.06$  (normals); the horizontal projection showed a similar separation ( $0.68$  and  $0.77$  vs  $0.23$  and  $-0.04$ ). 3D VG elevation (from the XY plane) differed by only  $\sim 3^\circ$  between DCM and DCM-I but by around  $\sim 30^\circ$  relative to HCM and  $\sim 40^\circ$  relative to normals (See Table S2 for full statistics). Figure 6 shows vectorcardiogram appearances of a representative patient from each group.

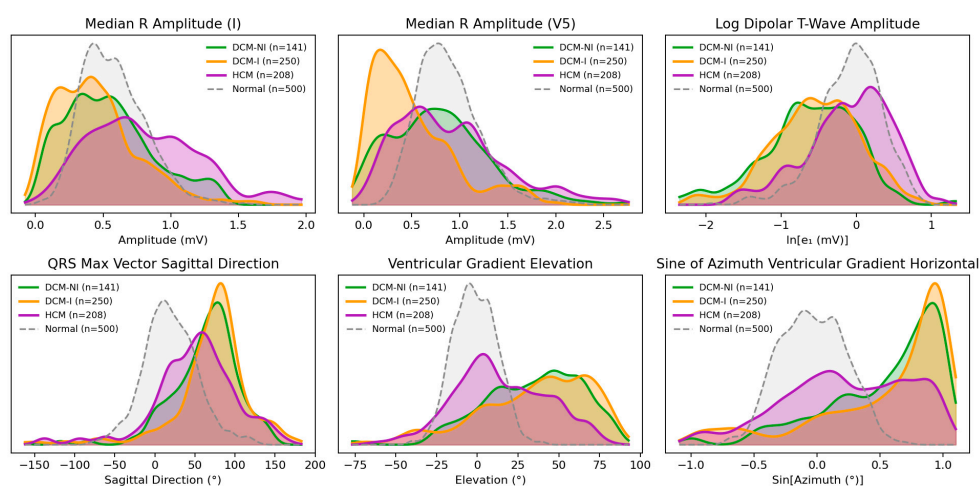


**Figure 5.** Kernel Density Estimate (KDE) plots of six ECG-derived features between non-ischemic DCM (DCM-NI), ischemic DCM (DCM-I), hypertrophic cardiomyopathy (HCM), and 500 electrically normal ECGs.

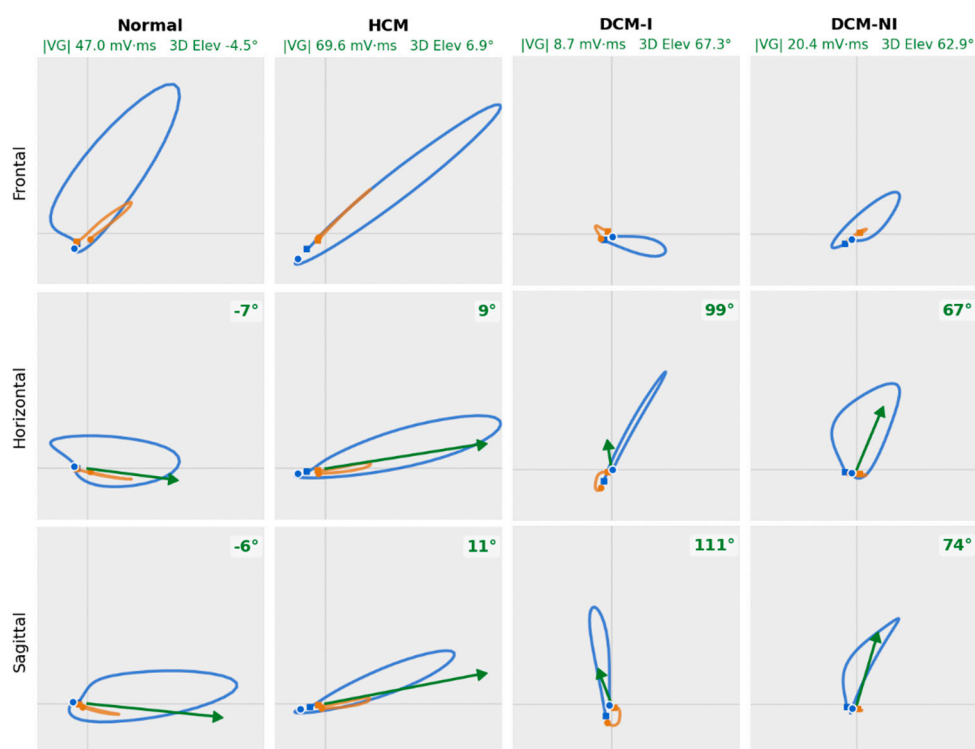


**Figure 6.** Four vectorcardiogram appearances for representative normal, HCM, DCM-I, and DCM-NI patients. The QRS loop is in blue, and the T loop is in orange. VG stands for ventricular gradient. The VG vector is marked in green for the horizontal and sagittal projections, and was not featured for the frontal view, as the standard QRS and T axes from the frontal view were not significant. The length of the VG vector is the magnitude of the projection on the shown view. The HCM patient shows larger loops, with slightly larger VG azimuths in comparison to the normal patient. Both DCM patients show loops smaller in amplitude in all projections, accompanied by small amplitude VG vectors with far higher 3D elevation and higher azimuth angles within the horizontal and sagittal projections.

### 3.3. Classifier Performance

Multivariate logistic regression and XGBoost models were trained on the complete feature set for HCM and DCM classification. Due to a lower sample size, only fifteen representative ECG features (nine amplitude, one duration, and five VCG) were inputted into the LR and XGBoost for HOCM vs HNCM. Performance metrics are displayed in Table 3. The receiver operating characteristic (ROC) curves are shown in Figure 7.

**Table 3.** Performance summary for binary ECG-based classifiers. Metrics are reported as mean across 5-fold cross-validation. Sensitivity and specificity are calculated at the Youden's J statistic threshold.

Task	AUC-ROC	AUC-PRC	Sensitivity	Specificity
<b>Logistic Regression</b>				
HCM vs DCM-NI	0.90	0.93	0.78	0.88
HCM vs DCM-I	0.92	0.92	0.83	0.88
HOCM vs HNCM	0.75	0.88	0.74	0.73
<b>XGBoost</b>				
HCM vs DCM-NI	0.90	0.92	0.87	0.81
HCM vs DCM-I	0.91	0.90	0.79	0.92
HOCM vs HNCM	0.81	0.92	0.69	0.85

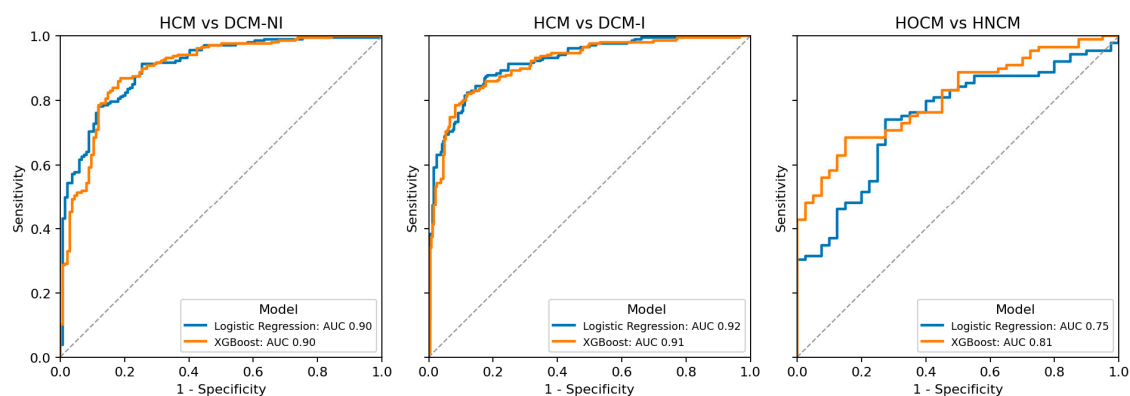


**Figure 7.** Pooled out-of-fold receiver operating characteristic (ROC) curves for each task and model type in the internal validation cohort. Each ROC curve plots sensitivity (true positive rate) against 1-specificity (false positive rate). AUC is the area under the curve.

## 4. Discussion

In our study, classifiers built solely from electrocardiogram input were developed to distinguish hypertrophic cardiomyopathy and dilated cardiomyopathy. Some conditions were easier to distinguish, including HCM as a whole versus ischemic or non-ischemic dilated cardiomyopathy (AUC-ROC 0.92 and 0.90), while detecting obstruction with ECG was more challenging (AUC-ROC 0.81 with XGBoost). The ECG features tested included a combination of lead-specific amplitude and

Fourier-based features, global interval/duration features, and vectorcardiogram-derived spatial features.

#### 4.1. General Cardiomyopathy Analysis

Demographically, non-ischemic DCM (DCM-NI) patients were younger by a median of over 11 years in comparison to DCM-I and HCM, while both ischemic and non-ischemic DCM were near 80% male, in comparison to ~46% of HCM patients. These demographics align with the EuroHeart Failure Survey II, which also found that DCM was more prevalent in males than females [23]. QRS amplitudes were consistently low in DCM, findings frequently observed in non-ischemic DCM and often linked to myocardial fibrosis on cardiac MRI [24]. In ischemic DCM, precordial R-wave amplitudes were even lower, consistent with the loss of anterior forces from infarct scar [25,26]. Uncorrected (rate-dependent) repolarization durations were shorter in DCM-NI, and DCM-NI also showed higher heart rates with more than twice the prevalence of sinus tachycardia compared with DCM-I and HCM. The T-index (upstroke/downstroke) was also higher in DCM-NI. Using a prominence-based delineator, the T-end is anchored to the right-hand base of the T peak (the adjacent minimum on the descending limb). When the TP interval shortens or the baseline rises (due to more frequent sinus tachycardia and a lower median RR interval), the upcoming P-wave elevates that minimum and shifts the base earlier, possibly shortening the T-wave downstroke. We therefore interpret T-index cautiously; this is unlikely to affect VCG orientation results, which depend on the higher-amplitude mid-T portion rather than the terminal tail.

VCG geometry revealed that both ischemic and non-ischemic DCM exhibited right-posterior orientation shifts of the ventricular gradient (VG) and more negative T-vector angles, while HCM preserved a more leftward VG but demonstrated larger and more complex and spatially non-planar T-loops. The similarity between non-ischemic and ischemic DCM in these VCG angles suggests that global ventricular dilatation and conduction delay, rather than the presence of an infarct scar, dominate the three-dimensional orientation of electrical activation in dilated cardiomyopathy.

#### 4.2. HCM Subtype Analysis

While harder to differentiate on ECG, several distinctions were found between obstructive and non-obstructive HCM: Through lead-amplitude analysis, HOCM consistently displayed more positive electrical activity on the left leads, while HNCM displayed the opposite. The prominent left-leaning electrical activity may be originating from hypertrophy severe enough to cause the obstructive physiology, which may explain the amplified electrical signals coming from the left side of the myocardium. At the same time, left ventricular hypertrophy alone was suggested by Savage et al. to be insufficient in determining the LVOT gradient [27]. Indeed, we note that in our cohort, the presence of left ventricular hypertrophy was not statistically significant ( $P = .59$ ) and only differed ~5% between HOCM and HNCM. This can also suggest another reason for the stronger left-lateral depolarization observed in HOCM. Guo et al. found the same overall correlation with HOCM having larger R-wave amplitudes in left leads and larger S-wave amplitudes in right leads [12]. They used the amplitude of the S wave in lead V1 (SV1) as one of two variables in a logistic regression model classifying HOCM, which we also found to be larger in HOCM patients. However, the duration of the P-wave, the other variable used in their model, in our cohort was longer in HNCM patients, while their study indicates the opposite effect. No prior study has used VCG-derived features to discriminate HOCM from HNCM. We found HNCM to have larger non-dipolar QRS components in comparison to dipolar components, suggesting that their depolarization are less planar and spatially more dispersed than HOCM. Further research is needed here.

To the best of our knowledge, all studies involved in any form of ECG cardiomyopathy diagnosis utilize non-public proprietary data, and thus, it can be increasingly difficult for other researchers without access to reproduce or create their own findings. This study uses only publicly available MIMIC-IV data and provides a reproducible framework for the use of open-source hospital

data and signal-processing with machine learning. We also provide clinically interpretable features in VCG analysis that link to cardiac anatomy.

#### 4.3. Limitations and Future Directions

Only inpatient data were included from the single-center Beth Israel Deaconess Medical Center. Inclusion of outpatient data may improve results. HOCM was more prevalent than HNCM in our cohort, likely due to echocardiogram-verified LVOTO being more common in an inpatient setting. With the use of the MIMIC-IV database, all data relies on the accuracy and quality of the project's diagnostic labels. This includes the validity of MIMIC's machine-generated ECG reports, which were used to exclude patients with paced rhythms and identify patients with atrial fibrillation or other categorical features. The accuracy of the diagnosis was confirmed by a large language model, and while the model extracted reliable results visibly (which are also public), large AI models can still hallucinate on occasion. Research with open-source data is confined to the information provided in the project, and many reliable HCM and DCM phenotype labels were not available. We could not include morphological HCM phenotypes, such as septal or apical HCM, into our analysis due to limited, reliable sample sizes. We did not have enough information to subtype ischemic dilated cardiomyopathy either. With further labels, one can implement the provided workflow to differentiate diastolic dysfunction physiology in HCM from DCM or other relevant phenotype combinations.

## 5. Conclusions

We provide the first framework to explore different cardiomyopathy presentations using open-source electrocardiograms. Our analysis combined standard ECG amplitude and duration features with more advanced signal processing and spatial vectorcardiography. We provide statistically significant features in detecting obstruction in hypertrophic cardiomyopathy, such as higher positive amplitudes in left-facing leads, along with more planar spatial depolarization. We confirm findings from prior studies, which conclude lower QRS amplitudes and higher QRS durations in DCM-NI and DCM-I patients. HCM displays spatially larger and more complex T-waves, while DCM-NI and DCM-I share abnormal QRS and T vector angles pointing towards the right ventricle. Finally, we developed an XGBoost model with an AUC-ROC of 0.81 to detect obstruction in HCM, and logistic regression models with an AUC-ROC of 0.92 and 0.90 distinguishing HCM from ischemic and non-ischemic DCM.

**Supplementary Materials:** The following supporting information can be downloaded at the website of this paper posted on Preprints.org. Table S1: ECG variables that differ significantly ( $p < 0.05$ ) between obstructive and non-obstructive HCM. Table S2: Descriptive statistics for all ECG features across HCM and DCM groups.

**Author Contributions:** Conceptualization, A.A., and A.R.; data curation, A.A.; formal analysis, A.A.; investigation, A.A.; methodology, A.A.; resources, A.A.; software, A.A.; supervision, A.R.; validation, A.A., and A.R.; visualization, A.A.; writing—original draft, A.A.; writing—review and editing, A.A., and A.R. All authors have read and agreed to the published version of the manuscript.

**Funding:** This research received no external funding.

**Data Availability Statement:** The code and scripts used to generate the results of this study are openly available at the GitHub repository: <https://github.com/againh3x/ECGcardiomyopathy>. The data used is within the open-source MIMIC-IV, MIMIC-IV-ECG, and MIMIC-IV-Note modules on PhysioNet. Because access to MIMIC-IV is restricted under a data-use agreement that protects patient privacy, raw or pre-processed patient-level data cannot be redistributed in the attached GitHub repository. Interested researchers can obtain the same data free of charge by completing the data-use certification on PhysioNet. MIMIC-IV-ECG is fully open-access. The project containing GPT-4.1 diagnosis labels corresponding to the admission ID and relevant quotes is currently under review for credentialed access.

**Acknowledgments:** We gratefully acknowledge Jason W. Fleischer and Amir Reza Vazifeh of Princeton University for valuable discussions and insights that contributed to this work.

**Conflicts of Interest:** The authors declare no conflicts of interest.

## Abbreviations

The following abbreviations are used in this manuscript:

A-ECG	Advanced electrocardiogram
AUC	Area under curve
AUC-ROC	Area under the receiver operating characteristic curve
AUC-PR	Area under the precision-recall curve
CM	Cardiomyopathy
DCM	Dilated cardiomyopathy
DCM-I	Dilated ischemic cardiomyopathy
DCM-NI	Dilated non-ischemic cardiomyopathy
ECG	Electrocardiogram
HCM	Hypertrophic cardiomyopathy
HNCM	Hypertrophic non-obstructive cardiomyopathy
HOCM	Hypertrophic obstructive cardiomyopathy
ICD	International Classification of Diseases
ICM	Ischemic cardiomyopathy
IQR	Interquartile range
LR	Logistic regression
LV	Left ventricle
LVOTO	Left ventricular outflow tract obstruction
ML	Machine learning
VCG	Vectorcardiogram
VG	Ventricular gradient
WFDB	Waveform Database Software Package

## References

1. Ciarambino, T.; Menna, G.; Sansone, G.; Giordano, M. Cardiomyopathies: An overview. *Int. J. Mol. Sci.* **2021**, *22*, 7722. DOI: 10.3390/ijms22147722.
2. Ashley, E.A.; Niebauer, J. *Cardiology Explained*; Remedica: London, UK, **2004**; pp. 15-34.
3. Captur, G.; Manisty, C.H.; Raman, B.; et al. Maximal wall thickness measurement in hypertrophic cardiomyopathy: biomarker variability and its impact on clinical care. *JACC Cardiovasc. Imaging* **2021**, *14*, 2123-2134. DOI: 10.1016/j.jcmg.2021.03.032.
4. Nasimov, R.; Nasimova, N.; Botirjon, K.; Abdullayev, M. Deep-Learning Algorithm for Classifying Dilated and Hypertrophic Cardiomyopathy in Transport Workers. In *Lecture Notes in Computer Science*; Springer: Cham, Switzerland, **2023**; pp. 218-230. DOI: 10.1007/978-3-031-30258-9\_19.
5. Zhou, M.; Deng, Y.; Liu, Y.; Su, X.; Zeng, X. Echocardiography-based machine-learning algorithm for distinguishing ischaemic from dilated cardiomyopathy. *BMC Cardiovasc. Disord.* **2023**, *23*, 215. DOI: 10.1186/s12872-023-03520-4.
6. Ko, W.Y.; Siontis, K.C.; Attia, Z.I.; Carter, R.E.; Kapa, S.; Ommen, S.R.; et al. Detection of hypertrophic cardiomyopathy with a convolutional-neural-network-enabled electrocardiogram. *J. Am. Coll. Cardiol.* **2020**, *75*, 722-733. DOI: 10.1016/j.jacc.2019.12.030.
7. Kokubo, T.; Koderia, S.; Sawano, S.; Katsushika, S.; Nakamoto, M.; Takeuchi, H.; et al. Automatic detection of left-ventricular dilatation and hypertrophy from electrocardiograms using deep learning. *Int. Heart J.* **2022**, *63*, 939-947. DOI: 10.1536/ihj.22-132.

8. Bacharova, L.; Kollarova, M.; Bezak, B.; Bohm, A. Left-ventricular hypertrophy and ventricular tachyarrhythmia: The role of biomarkers. *Int. J. Mol. Sci.* **2023**, *24*, 3881. DOI: 10.3390/ijms24043881.
9. Hughes, R.K.; Thornton, G.D.; Malcolmson, J.W.; et al. Accurate diagnosis of apical hypertrophic cardiomyopathy using explainable advanced electrocardiogram analysis. *Europace* **2024**, *26*, euae093. DOI: 10.1093/europace/euae093.
10. Maron, M.S.; Olivotto, I.; Betocchi, S.; Casey, S.A.; Losi, M.A.; Cecchi, F.; Maron, B.J. Effect of left ventricular outflow tract obstruction on clinical outcome in hypertrophic cardiomyopathy. *N. Engl. J. Med.* **2003**, *348*, 295-303. DOI: 10.1056/NEJMoa021332.
11. Nourani, M.; Mirzaie, M.; Sadr-Ameli, M.A.; Fazelifar, A.; Haghjoo, M. Role of surface electrocardiography in differentiation between obstructive and non-obstructive hypertrophic cardiomyopathy. *J. Tehran Heart Cent.* **2023**, *18*, 46-51. DOI: 10.18502/jthc.v18i1.12581.
12. Guo, C.; Zhang, Y.; Liu, Y.; et al. Development and external validation of an ECG-based model for discriminating obstructive versus non-obstructive hypertrophic cardiomyopathy. *Eur. Heart J. Digit. Health* **2023**, *4*, 356-365. DOI: 10.1093/ehjdh/ztd042.
13. Johnson, A.E.W.; Bulgarelli, L.; Pollard, T.J.; et al. MIMIC-IV, a freely accessible electronic health-record database. *Sci. Data* **2023**, *10*, 1-11. DOI: 10.1038/s41597-022-01899-x.
14. Johnson, A.E.W.; Bulgarelli, L.; Pollard, T.J.; et al. MIMIC-IV (version 3.0); PhysioNet: Cambridge, MA, USA, **2024**. DOI: 10.13026/hxp0-hg59.
15. Goldberger, A.L.; Amaral, L.A.N.; Glass, L.; et al. PhysioBank, PhysioToolkit, and PhysioNet: Components of a new research resource for complex physiologic signals. *Circulation* **2000**, *101*, e215-e220. DOI: 10.1161/01.CIR.101.23.e215.
16. Gow, B.; Pollard, T.; Nathanson, L.A.; et al. MIMIC-IV-ECG: Diagnostic electrocardiogram matched subset (version 1.0); PhysioNet: Cambridge, MA, USA, **2023**. DOI: 10.13026/4nqg-sb35.
17. Johnson, A.E.W.; Pollard, T.; Horng, S.; Celi, L.A.; Mark, R. MIMIC-IV-Note: Deidentified free-text clinical notes (version 2.2); PhysioNet: Cambridge, MA, USA, **2023**. DOI: 10.13026/1n74-ne17.
18. OpenAI. GPT-4.1 (Large Language Model) [Computer software]. Available online: <https://platform.openai.com/> (accessed on 9 April 2025).
19. Xie, C.; McCullum, L.; Johnson, A.; et al. Waveform Database Software Package (WFDB) for Python (version 4.1.0); PhysioNet: Cambridge, MA, USA, **2023**. DOI: 10.13026/9njx-6322.
20. Makowski, D.; Pham, T.; Lau, Z.J.; Brammer, J.C.; Lespinasse, F.; Pham, H.; et al. NeuroKit2: A Python toolbox for neurophysiological signal processing. *Behav. Res. Methods* **2021**, *53*, 1689-1696. DOI: 10.3758/s13428-020-01516-y.
21. Emrich, J.; Gargano, A.; Koka, T.; Muma, M. Physiology-Informed ECG Delineation Based on Peak Prominence. In Proceedings of the 32nd European Signal Processing Conference (EUSIPCO), Lyon, France, 26-30 August **2024**; pp. 1402-1406.
22. Kors, J.A.; van Herpen, G.; Sittig, A.C.; van Bommel, J.H. Reconstruction of the Frank vectorcardiogram from standard electrocardiographic leads: Diagnostic comparison of different methods. *Eur. Heart J.* **1990**, *11*, 1083-1092.
23. Nieminen, M.S.; Harjola, V.P.; Hochadel, M.; Drexler, H.; Komajda, M.; Brutsaert, D.; et al. Gender-related differences in patients presenting with acute heart failure: EuroHeart Failure Survey II. *Eur. J. Heart Fail.* **2008**, *10*, 140-148. DOI: 10.1016/j.ejheart.2007.12.012.
24. Crescenzi, C.; Silvetti, E.; Romeo, F.; Martino, A.; Bressi, E.; Panattoni, G.; et al. The electrocardiogram in non-ischaemic dilated cardiomyopathy. *Eur. Heart J. Suppl.* **2023**, *25* (Suppl. C), C179-C184. DOI: 10.1093/eurheartjsupp/suad043.
25. Kurisu, S.; Iwasaki, T.; Watanabe, N.; et al. Poor R-wave progression and myocardial infarct size after anterior myocardial infarction in the coronary intervention era. *Int. J. Cardiol. Heart Vasc.* **2015**, *7*, 106-109. DOI: 10.1016/j.ijcha.2014.09.002.

26. Rijnierse, M.T.; Verouden, N.J.; de Winter, R.J. Precordial R-wave reappearance predicting infarct size and myocardial recovery after acute STEMI. *Neth. Heart J.* **2012**, *20*, 326-329. DOI: 10.1007/s12471-011-0162-9.
27. Savage, D.D.; Seides, S.F.; Clark, C.E.; Henry, W.L.; Maron, B.J.; Robinson, F.C.; et al. Electrocardiographic findings in patients with obstructive and nonobstructive hypertrophic cardiomyopathy. *Circulation* **1978**, *58*, 402-408. DOI: 10.1161/01.CIR.58.3.402.

**Disclaimer/Publisher's Note:** The statements, opinions and data contained in all publications are solely those of the individual author(s) and contributor(s) and not of MDPI and/or the editor(s). MDPI and/or the editor(s) disclaim responsibility for any injury to people or property resulting from any ideas, methods, instructions or products referred to in the content.